Kenaf Bast Fiber Bundle–Reinforced Unsaturated Polyester Composites. IV: Effects of Fiber Loadings and Aspect Ratios on Composite Tensile Properties

Yicheng Du Jilei Zhang Jaesang Yu Thomas E. Lacy, Jr.
Yibin Xue Hossein Toghiani Mark F. Horstemeyer
Charles U. Pittman, Jr.

Abstract

Mechanically retted short kenaf bast fiber bundle (KBFB)–reinforced unsaturated polyester (UPE) composites were fabricated. The effects of fiber loadings and aspect ratios on composite tensile properties were evaluated experimentally and theoretically. Tensile properties of KBFBs and the neat cured UPE were determined, and kenaf-UPE shear bonding strengths were measured. These measured properties were used to predict the tensile properties of the short KBFB-reinforced UPE composites using classical models in micromechanics. Theoretical tensile moduli predicted by Halpin–Tsai, Mori–Tanaka, and Self-Consistent models were in good agreement with experimental results. Theoretical tensile strengths predicted by the Kelly–Tyson model correlated well with experimental results at high fiber aspect ratios. Both composite tensile moduli and strengths increased consistently with increasing fiber loadings up to 75 percent (vol/vol).

Kenaf bast fiber bundles (KBFBs) have the potential to replace petroleum-based or glass fibers for fiber-reinforced composite applications due to their low density, high specific strength and stiffness, low cost, reduced wear on the processing equipment, renewability, and biodegradability. Recently, natural fiber–reinforced thermoplastics have been widely used for automobile interior parts (Holbery and Houston 2006). If natural fiber–reinforced thermoset polymer composites are desired for semi-structural or exterior automotive component applications, their mechanical properties need to be predictable and designable.

Fiber-reinforced polymer composite tensile stiffness and strength depend on the mechanical properties of the reinforcing fibers and the matrix, fiber volume fraction, fiber orientation and dispersion form in the matrix, fiber aspect ratio, and fiber–matrix interfacial shear bonding strength. The effect of fiber aspect ratios on composite tensile moduli is also related to the tensile moduli ratio of fiber to matrix (Agarwal et al. 2006). Table 1 chronolog-

The authors are, respectively, former graduate student and Professor, Dept. of Forest Products (yicheng.du@utoronto.ca, jZhang@cfr.msstate.edu), and Graduate Student and Associate Professor, Dept. of Aerospace Engineering (jy125@msstate.edu, lacy@ae.msstate.edu), Mississippi State Univ., Mississippi State; Assistant Professor, Dept. of Mechanical and Aerospace Engineering, Utah State Univ., Logan (anna.xue@usu.edu); Associate Professor, Dept. of Chemical Engineering (hossein@che.msstate.edu), Professor, Dept. of Mechanical Engineering (mfhorst@cavs.msstate.edu), and Professor, Dept. of Chemistry (CPittman@chemistry.msstate.edu), Mississippi State Univ., Mississippi State. This report was prepared as an account of work sponsored by an agency of the US government. Approved for publication as Journal Article no. FP 561 of the Forest and Wildlife Research Center, Mississippi State Univ. This paper was received for publication in May 2010. Article no. 10-00006.

Forest Prod. J. 60(7/8):582–591.

Table 1.—Widely cited classical models for predicting tensile moduli and strengths for fiber-reinforced composites.

Model	Fiber form	Reference
Young's modulus		
Rule of mixtures	Unidirectional; continuous	cf. Agarwal et al. 2006
Modified rule of mixtures	Randomly; long straight thin fibers	Cox 1952
Nielsen–Chen	Random; fiber length above critical length	Nielsen and Chen 1968
Halpin–Tsai	Unidirectional; discontinuous	Halpin 1969
Modified Halpin–Tsai	Unidirectional; discontinuous;	Nielsen 1970
Mori–Tanaka	Unidirectional or randomly oriented; continuous or discontinuous	Mori and Tanaka 1973
Self-Consistent	Unidirectional or randomly oriented; continuous or discontinuous	Hill 1965
Tensile strength		
Rule of mixtures	Unidirectional; continuous;	cf. Agarwal et al. 2006
Kelly–Tyson	Unidirectional; discontinuous	Kelly and Tyson 1965
Bowyer–Bader	Unidirectional or randomly; discontinuous	Bowyer and Bader 1972

ically summarizes widely used empirical and numerical models, which have been frequently used over several decades to predict man-made fiber–reinforced composite tensile properties.

These models have been used to describe natural fiber–reinforced thermoplastic or thermoset polymer composite tensile properties. Joseph et al. (2003) studied tensile moduli and tensile strengths of poly[methylene poly(phenyl isocyanate)]–treated sisal fiber–reinforced polypropylene composites with fiber loadings from 0 to 40 percent (wt/wt). Both composite tensile moduli and tensile strengths increased with increasing fiber loadings. Experimentally obtained Young's moduli and tensile strengths were compared with the values predicted by the rule of mixtures (ROM; cf. Agarwal et al. 2006), the modified rule of mixtures (m-ROM; Cox 1952), the Bowyer–Bader (Bowyer and Bader 1972), and the Hirsch (1962) models. The m-ROM was the best model for predicting tensile strengths among these models (Joseph et al. 2003). Composite Young's moduli were higher than the values predicted by the ROM lower bound and the Hirsch and the Bowyer–Bader models and were lower than theoretical values predicted by the ROM upper bound, which is used for predicting unidirectional continuous fiber–reinforced composite tensile moduli.

Baiardo et al. (2004) fabricated flax fiber–reinforced polyester composites with fiber volume fractions ranging from 1 to 37.5 percent (vol/vol). Experimental moduli were predicted well by the m-ROM (Cox 1952) with fiber loadings between 12.5 and 37.5 percent (vol/vol). The tensile strengths, however, decreased when the fiber loading was higher than 12.5 percent (vol/vol) due to poor fiber–matrix adhesion.

Xue et al. (2007) studied tensile and flexural properties of aspen fiber–polypropylene composites with 0 to 60 percent (wt/wt) fiber loadings. Tensile moduli increased as fiber loadings increased from 0 to 60 percent (wt/wt), while tensile strengths increased with increasing fiber loadings from 0 to 50 percent (wt/wt) and then decreased. Composite tensile moduli calculated by the Halpin–Tsai (Halpin 1969) and the modified Nielsen–Chen (Nielsen and Chen 1968) models correlated well with the experimental data for fiber loadings from 0 to 30 percent (wt/wt), but were 22, 13, and 34 percent lower than the experimental results with 40, 50, and 60 percent (wt/wt) fiber, respectively.

Haneefa et al. (2008) studied the mechanical properties of short banana/glass hybrid fiber–reinforced polystyrene composites with 0 to 30 percent (wt/wt) fiber loadings. Tensile moduli and strengths improved with increasing fiber loadings. Experimental tensile properties agreed well with theoretical values predicted by the lower bound of the ROM, the Hirsch (1962), the Halpin–Tsai (Halpin 1969), the modified Halpin–Tsai (Nielsen 1970), and the Bowyer–Bader (Bowyer and Bader 1972) models. Upper bound ROM estimates did not correlate well with experimental data.

Devi et al. (1997) studied pineapple leaf fiber–reinforced polyester composites reinforced by 10 to 40 percent (wt/wt) of fibers with fiber lengths between 5 and 40 mm. Both Young's moduli and tensile strengths increased with increasing fiber loadings. The maximum tensile properties were found with 30-mm-long fiber. When the fiber length was increased to 40 mm, the reductions of Young's modulus and tensile strength were 14 and 27 percent, respectively.

Takagi and Ichihara (2004) reported the effects of fiber length and loading on bamboo fiber–reinforced starch resin composite tensile and flexural strengths. Tensile and flexural strengths consistently increased with larger fiber loadings between 0 and 50 percent (wt/wt) with one exception of the flexural strength decreased at 50 percent (wt/wt). The tensile and flexural strengths also increased as the fiber lengths were increased from 4 to 25 mm (4 to 125 in aspect ratios), and asymptotically approached the maximum values.

Shibata et al. (2006) used the m-ROM (Cox 1952) to predict flexural properties of short kenaf fiber–reinforced starch polymer composites with 0 to 67.5 percent (vol/vol) fiber loadings. In addition, the fiber lengths were varied from 1.8 to 10.7 mm (fiber aspect ratios, 15 to 89). Flexural moduli increased with increasing fiber loadings up to 60 percent (vol/vol). The maximum flexural strength was reached when the fiber loading was near to 40 percent (vol/vol). Flexural moduli and strengths improved as fiber lengths increased. Flexural moduli closely matched theoretical values predicted by Cox's model (1952).

Liu et al. (2007) reported the storage moduli of kenaf fiber–reinforced soy-based biocomposites with fiber volumes of 0 to 53 percent (vol/vol) and lengths of 2, 6, 25, and 50 mm. Moduli increased almost linearly with increasing fiber loadings from 0 to 53 percent (vol/vol). A significant modulus increase (28%) occurred as the fiber length increased from 2 to 6 mm. Only a small modulus increase (5%) was found as the fiber length increased from 6 to 25 mm. The modulus remained almost the same as the fiber length increased from 25 to 50 mm.

Ochi (2008) studied the tensile and flexural properties of biodegradable kenaf–poly-lactic acid composites with fiber

loadings ranged from 30 to 70 percent (vol/vol). Both the tensile and flexural strengths increased linearly with increasing fiber loadings up to 50 percent (vol/vol). The experimental strengths were about 70 percent of the theoretical values calculated by the ROM at lower fiber loadings (30% and 50%, vol/vol), and this percentage decreased to 54 percent when the fiber loading increased to 70 percent (vol/vol).

Özturk (2010) studied the effect of fiber loading (19%, 28%, 36%, 43%, 52%, and 62%, vol/vol) on the kenaf fiber–reinforced phenol–formaldehyde composite tensile, flexural, and impact strengths. The highest properties were achieved for the composite with a 43 percent (vol/vol) fiber loading.

Abu Bakar et al. (2010) compared the flexural properties of untreated and alkali-treated kenaf fiber–reinforced epoxy composites with fiber loadings ranging from 0 to 25 percent (wt/wt). The highest flexural strength and modulus for untreated kenaf fiber–reinforced epoxy composites were obtained when the fiber loadings were 10 and 15 percent (wt/wt), respectively. The alkali treatment ensured the flexural strength and modulus increased with increasing fiber loadings up to 25 percent (wt/wt).

In the literature of the family of natural fiber–reinforced polymer composites, the fiber length effect on composite mechanical properties could be satisfactorily described by the classical models. However, the effect of fiber loadings on composite mechanical properties differs because the assumption of perfect fiber–matrix bonding for those classical models is not appropriate for natural fiber–reinforced polymer composites, especially at higher fiber loading levels. This induces the presence of ''the critical fiber loading,'' at which the composite mechanical property begins to decrease even if the fiber loading increases. This value differs in literature due to various composite fabrication methods and the use of interfacial bonding improvement. The objectives of this study were to (1) investigate fiber aspect ratio and loading effects on tensile properties of kenaf–unsaturated polyester (UPE) composites fabricated by the process developed in previous study (Du et al. 2010), (2) obtain tensile and shear bonding properties of KBFB and the UPE matrix and their shear bonding strength properties, and (3) attempt to use available empirical and analytic models to predict the tensile properties of short KBFB–reinforced UPE composites with fiber loadings up to 65 percent (wt/wt).

Materials and Methods

Materials

In this study, mechanically retted KBFBs, provided by Kengro Corporation, were used as reinforcing fibers. The average diameter of these KBFBs was 78.6 μm. The UPE (Aropol Q-6585), provided by Ashland Chemical Company, was used as the matrix polymer. The diluent, styrene, and the catalyst, *t*-butyl perbenzoate, were purchased from Fisher Scientific Inc. Methyl ethyl ketone peroxide, purchased from Sigma-Aldrich Corporation, and cobalt naphthenate, purchased from Fisher Scientific Inc., were used as a second catalyst system. A polyvinyl acetate (PVAc) water emulsion (solid content, 46%) provided by Tailored Chemical was used as the mat preforming binder.

Experimental

KBFB tensile properties.—Short KBFB samples were randomly cut from long mechanically retted KBFBs. Twenty replicates were used. Tensile specimens were prepared using a previously published method (Du et al. 2008). These specimens were dried at 103°C for 3 hours to assure the moisture content of these KBFB specimens was negligible. After drying, each specimen was sealed immediately in individual plastic bags to avoid moisture uptake. KBFB tensile properties were obtained on a micromechanical testing machine according to ASTM Standard C1557-03 (ASTM International 2003).

Cured UPE tensile properties.—The UPE resin was mixed with a stirrer into the following formulation (by weight): 100 parts of UPE, 15 parts of styrene, 0.5 part of cobalt naphthenate, and 1.0 part of methyl ethyl ketone peroxide. The mixture was poured into a mold and cured into bars at room temperature for 24 hours followed by postcuring at 80°C for 3 hours. After cooling, the bars were cut into eight strips with nominal dimensions of 165 by 19 by 6.4 mm using a band saw. They were shaped into dog-bone tensile specimens using a computer numerical controlled machine. All tensile specimens were tested on an Instron 5869 universal testing machine under displacement control conditions in accordance with ASTM Standard D638-03 (ASTM International 2004). Tensile strains were recorded by an Instron 2630–100 series extensometer.

KBFB–UPE shear bonding strengths.—Eight specimens were prepared and tested. Kenaf strips (50 by 3 mm) were cut from kenaf bast fiber ribbons. One side of these strips at one end was smoothed by sand paper (120-grit). These strips were dried in an oven for 5 hours at 103°C to remove residual moisture. Shear specimens were prepared by pasting these kenaf strips onto cured 13 by 13 by 6.4-mm UPE blocks using a UPE resin paste mixed with the same formulation used in the UPE tensile specimens. These specimens were cured at a room temperature for 24 hours followed by postcuring at 80°C for 3 hours. A shear specimen schematic is shown in Figure 1. Testing was conducted on an Instron 5566 testing machine under displacement control conditions. Shear failure loads were recorded and shear bonding strengths were calculated using

$$\tau_{fm} = F/(LW) \tag{1}$$

where τ_{fm} is the fiber–matrix shear bonding strength, and *F,*

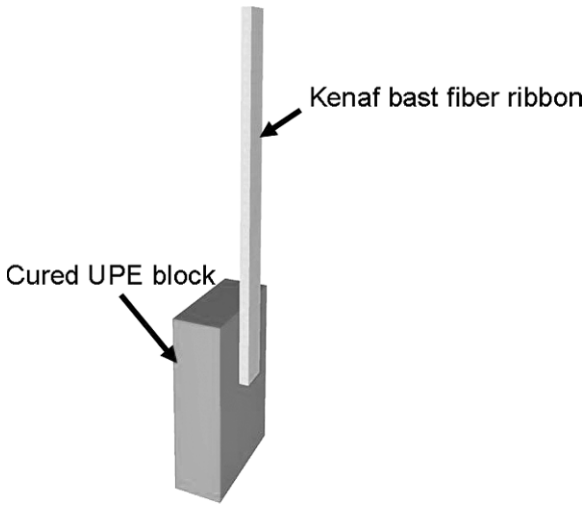

Figure 1.—A shear specimen schematic for fiber–matrix shear bonding strength testing.

L, and *W* are the failure load, overlap surface length, and width, respectively.

Composite tensile properties.—Three fixed fiber lengths were used: 1.72, 2.75, and 3.30 mm, equivalent to 22, 35, and 42 aspect ratios, respectively. At least two fiber loading levels were used at each aspect ratio. At least five replicates were tested at each fiber length and loading combination.

Short KBFBs were prepared by grinding long KBFBs in a Thomas Wiley mill (Model 4). The short KBFBs were divided into three batches by screening the ground short KBFBs using three different sieves. Fifty short KBFBs were randomly selected from each KBFB batch, and the average lengths of three KBFB batches were measured using a microscope. Figure 2 shows the length distribution of each KBFB batch.

Composites were fabricated as previously described (Du et al. 2010). The UPE resin was prepared using 100 parts of UPE, 15 parts of styrene, and 1.5 parts of *t*-butyl perbenzoate catalyst by weight. Short KBFBs were made into preforms using the PVAc adhesive and were compounded with prescribed amounts of UPE resin. Five resin-infused preformed mats were stacked to assemble one prepreg. The prepregs were then compression molded to kenaf-PVAc-UPE (KPU) composites at 175°C under a pressure of 5 MPa. The KPU composite fiber loadings were calculated after the squeezed-out resin was sanded off.

Tensile specimens for tensile property testing were cut from 102 by 178-mm KPU composites and shaped to dog-bone specimens using a computer numerical controlled machine. Tensile testing was performed on an Instron 5869 universal testing machine under displacement control conditions according to ASTM Standard 638-03 (ASTM International 2004). The tensile strains were recorded by an Instron 2630-100 series extensometer.

Results and Discussion

Fiber and matrix tensile properties, and fiber–matrix shear properties

Table 2 summarizes the tensile properties of KBFBs and the neat cured UPE, and the fiber–matrix shear bonding strength. The average density of KBFBs was 0.806 g/cm^3 (tested at Micromeritics Analytical Services). Typical KBFB and cured UPE stress–strain curves are plotted in Figure 3. Figure 4 contains fracture surfaces of KBFB observed by scanning electron microscopy (SEM) and neat cured UPE tensile specimen. KBFBs clearly displayed brittle fiber breakage, and the UPE specimens all failed due to flat (cleavage) fracture. According to the stress–strain plots and fracture surfaces, both KBFBs and the UPE are considered to be brittle materials.

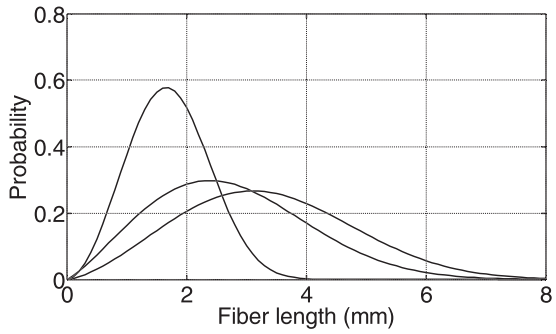

Figure 2.—Length distributions of three batches of reinforcing kenaf bast fiber bundle.

KBFB–UPE composites

Figures 5a and 5b show two SEM images of the composite tensile specimen fracture surfaces. Both fiber pullout and fiber breakage can be observed (Fig. 5a). The composites had a moderate degree of fiber–matrix interfacial bonding. The reinforcing fibers were mostly randomly aligned in a two-dimensional mat form (Fig. 5b).

The polymer matrix in the composite can be considered a polymer blend of the UPE and the PVAc. The PVAc (a fiber mat preforming binder) has a similar density, modulus of elasticity, and tensile strength as the UPE matrix (Table 2). The PVAc volume fraction is small in all cases (5.2% to 5.9l%, vol/vol). Therefore, the UPE properties were taken as the bulk matrix properties in the composite tensile property calculations. Fiber weight percentages in the composites were converted to volume percentages using the densities of KBFBs and UPE (Table 2).

Composite tensile moduli were predicted using the Halpin–Tsai (Halpin 1969), the m-ROM (Cox 1952), the Mori–Tanaka (Mori and Tanaka 1973), and the Self-Consistent (Hill 1965) models. The Halpin–Tsai model (Halpin 1969) for predicting the longitudinal and transverse stiffness of aligned short fiber–reinforced composites may be expressed as

$$\frac{E_l}{E_m} = \frac{1 + 2(l/d)\eta_l V_f}{1 - \eta_l V} \qquad \eta_l = \frac{(E_f/E_m) - 1}{(E_f/E_m) + 2(l/d)} \quad (2)$$

$$\frac{E_t}{E_m} = \frac{1 + 2\eta_t V_f}{1 - \eta_t V} \qquad \eta_t = \frac{(E_f/E_m) - 1}{(E_f/E_m) + 2} \quad (3)$$

where E_l and E_t are composite longitudinal and transverse moduli of a unidirectional short fiber–reinforced composite, η_l and η_t are the length efficiency factors, V_f and E_f are the fiber volume fraction and the fiber tensile modulus, E_m is the matrix tensile modulus, and l/d is the fiber aspect ratio. For cases in which short fibers are randomly oriented in a two-dimensional mat, the composite's modulus, E_c, can be computed using the following empirical equation (Agarwal et al. 2006):

$$E_c = \frac{3}{8}E_l + \frac{5}{8}E_t \quad (4)$$

Composite tensile modulus may also be calculated using the m-ROM (Cox 1952):

$$E_c = \eta_\theta \eta_l V_f E_f + (1 - V_f)E_m \quad (5)$$

$$\eta_l = 1 - \tanh[n(l/d)]/[n(l/d)] \quad (6)$$

$$n = \sqrt{\frac{2G_m}{E_f \ln(2R/d)}} \quad (7)$$

where η_l is the length efficiency factor and η_θ is the fiber orientation factor, which is assumed to be 0.33 for a two-dimensional random fiber composite (Cox 1952). KBFBs are assumed to be arranged in a square array, so $2R/d = [\pi/$

Table 2.—Physical and mechanical properties of kenaf and neat cured unsaturated polyester.

Properties	Data	COV (%)[a]	Source
Kenaf fiber bundle			
Density (g/cm^3)	0.806		Tested at Micromeritics Analytical Services
Elastic modulus (GPa)	19.2	24.6	Measured
Diameter (μm)	78.6	30.0	Measured
Strength (MPa)	260	19.6	Measured
Elongation (%)	1.22	23.6	Measured
Unsaturated polyester			
Density (g/cm^3)	1.18	0.75	Measured
Elastic modulus (GPa)	3.46	7.1	Measured
Tensile strength (MPa)	24.4	8.2	Measured
Elongation (%)	0.725	9.9	Measured
Poisson ratio	0.37		Pascault 2002
Shear modulus (GPa)	1.26		Calculated, $G = E/2(1 + \mu)$
Polyvinyl acetate			
Density (g/cm^3)	1.19		Brandrup and Immergut 1989
Elastic modulus (GPa)	1.28–2.26		Mark 2004
Tensile strength (MPa)	29.4–49.0		Mark 2004
Fiber–matrix			
Shear strength (MPa)	6.36	26.3	Measured
Critical length (mm)	1.61		Calculated, $L_c = \sigma_{uf} r/\tau_{um\text{-}f}$

[a] COV = coefficient of variation.

$(4V_f)]^{0.5}$. The matrix shear modulus G_m was estimated from

$$G_m = \frac{E_m}{2(1+\nu)} \tag{8}$$

where ν is the UPE's Poisson ratio, taken as 0.37 (Pascault et al. 2002).

The effective moduli of KBFB–UPE composites were also calculated using the classical Mori–Tanaka and Self-Consistent micromechanical models (cf. Mura 1991, Nemat-Nasser and Hori 1993, Qu and Cherkaoui 2006). Both of these effective medium approaches are based upon the Eshelby (1957) solution for the stress and strain fields inside and surrounding an ellipsoidal inclusion. They can be used to predict effective elastic properties for composites containing a variety of aligned or randomly oriented reinforcements (spheres, platelets, short fibers, continuous fibers, etc.) using the continuum-averaged stress and strain fields (cf. Hill 1965, Mori and Tanaka 1973, Benveniste 1987, Mura 1991, Nemat-Nasser and Hori 1993, Qu and Cherkaoui 2006). In the Mori–Tanaka method (Mori and Tanaka 1973, Benveniste 1987), it is assumed that a single ellipsoidal heterogeneity is embedded into an elastic matrix whose strain field has been perturbed by other heterogeneities in the system. The fourth-rank elastic stiffness tensor, $\bar{L}$, for an effective continuum with $(N-1)$ distinct aligned ellipsoidal heterogeneities may be expressed as

$$\bar{L} = \sum_{r=0}^{N} V_r L_r T_r \left[\sum_{n=0}^{N} V_n T_n \right]^{-1} \tag{9}$$

where $T_n = [I + S_n(M_0 L_n - I)]^{-1}$ is the fourth-rank local strain concentration tensor for the nth phase, S_n is the fourth-rank Eshelby tensor for the nth phase, L_n is the fourth-rank elastic stiffness tensor for the nth phase, V_n is the volume fraction of the nth phase, and M_0 is the fourth-rank elastic compliance tensor for the matrix (cf. Mura 1991, Nemat-Nasser and Hori 1993, Qu and Cherkaoui 2006). The Eshelby tensor (S_n) accounts for the influence of the aspect ratio/geometry of the nth heterogeneity on the local strain field. Eshelby tensors for specific reinforcement shapes (spheres, platelets, fibers, etc.) are readily available in the literature (cf. Mura 1991, Nemat-Nasser and Hori 1993, Qu and Cherkaoui 2006). In Equation 9, $n = 0$ is used to denote matrix properties. The fourth-rank effective compliance tensor, $\bar{M}$, may be determined by inverting the effective stiffness tensor (Eq. 9). After performing requisite orientation averaging to account for the effect of two-dimensional randomly oriented fibers on the calculated effective properties (Fisher 2002), the compliance tensor may be expressed as a 6×6 matrix using Voigt notation. The in-plane effective modulus for the composite may be expressed as

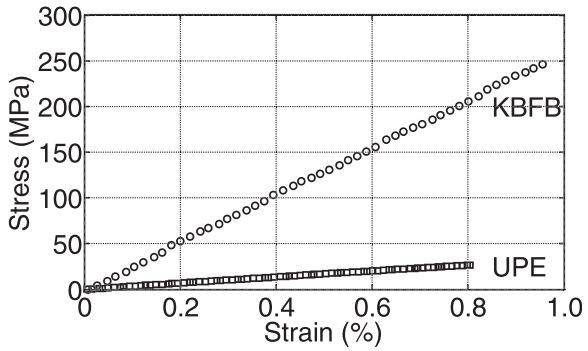

Figure 3.—Typical stress–strain plots for kenaf bast fiber bundle (KBFB) and unsaturated polyester (UPE) tensile specimens.

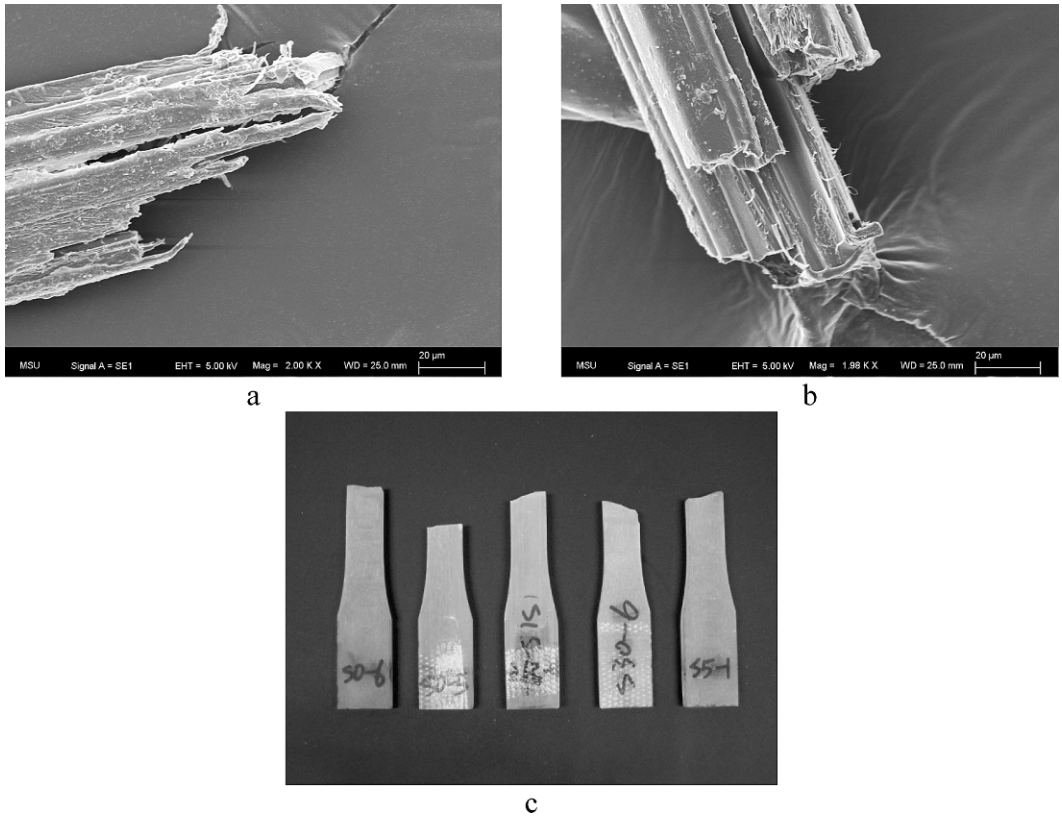

Figure 4.—Typical failure modes of kenaf bast fiber bundles (KBFBs) and the neat cured unsaturated polyester (UPE). (a and b) SEM fracture surfaces of representative KBFB tensile specimens. (c) Fracture surfaces of UPE tensile specimens.

$$E_c = \frac{1}{\bar{M}_{11}} \tag{10}$$

In the Self-Consistent method (Hill 1965), it is assumed that a single ellipsoidal heterogeneity is embedded into an elastic matrix whose (yet unknown) properties correspond to those of the effective continuum. Using the Self-Consistent approach, the fourth-rank stiffness tensor for the effective continuum may be expressed as (Qu and Cherkaoui 2006)

$$\bar{L} = L_0 + \sum_{r=1}^{N} V_r (L_r - L_0)\bar{T}_r \tag{11}$$

where $\bar{T}_r = [I + S_r \bar{L}^{-1}(L_r - \bar{L}^{-1})]^{-1}$ is the global strain concentration tensor. The effective stiffness tensor (Eq. 11) may be determined in an iterative fashion. The fourth-rank effective compliance tensor, $\bar{M}$, may be determined by inverting the effective stiffness tensor (Eq. 11), and the effective in-plane modulus for the composite may be determined in a fashion similar to that for the Mori–Tanaka method. Both the Mori–Tanaka and Self-Consistent methods account for the effect of weak interactions between adjacent fibers on the bulk composite properties. While these approaches are best suited for composites with $V_f < 0.5$, Mori–Tanaka and Self-Consistent estimates for E_c were developed in this study for comparison purposes. Similarly, Voigt upper bound and Reuss lower bound ROM estimates for E_c were also calculated in order to bound the range of elastic properties (cf. Agarwal et al. 2006), i.e.,

$$E_{cUPR} = V_f E_f + (1 - V_f)E_m \quad \text{(Voigt Upper Bound)} \tag{12}$$

$$E_{cLWR} = \frac{E_f E_m}{V_f E_m + (1 - V_f)E_f} \quad \text{(Reuss Lower Bound)} \tag{13}$$

The predicted tensile moduli by the Halpin–Tsai, m-ROM, Mori–Tanaka, and Self-Consistent models are plotted as a function of fiber loadings in Figure 6. The upper and lower bound ROM estimates for composite tensile moduli are also plotted for reference purposes; these models are best suited for predicting unidirectional continuous fiber–reinforced composite properties. Included in the figure are experimentally measured tensile moduli for KBFB composites. The relative errors between the predicted and experimental tensile moduli are summarized in Table 3. The tensile moduli predicted using the Halpin–Tsai, Mori–Tanaka, and Self-Consistent models captured the essential character of the experimental results, although a significant scatter in observed results exists.

The m-ROM significantly underestimated the experimental values. Baiardo et al. (2004) and Shibata et al. (2006) found good agreement between natural fiber–reinforced composite experimental tensile moduli and computed values by the m-ROM. Results from this study suggested Halpin–Tsai, Mori–Tanaka, and Self-Consistent models better approximated the measured data over the range of fiber loadings considered here.

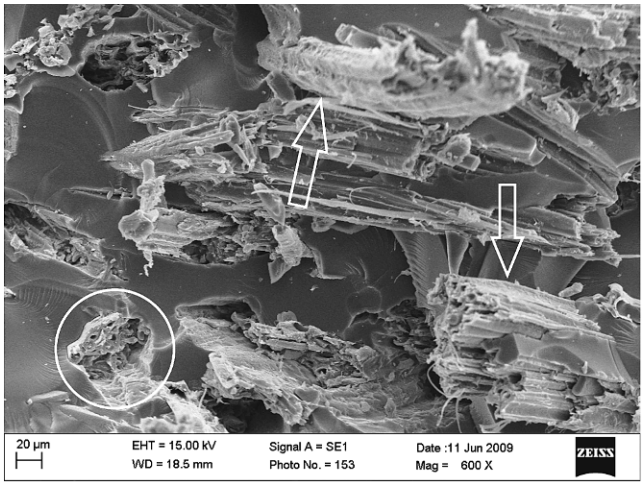

a

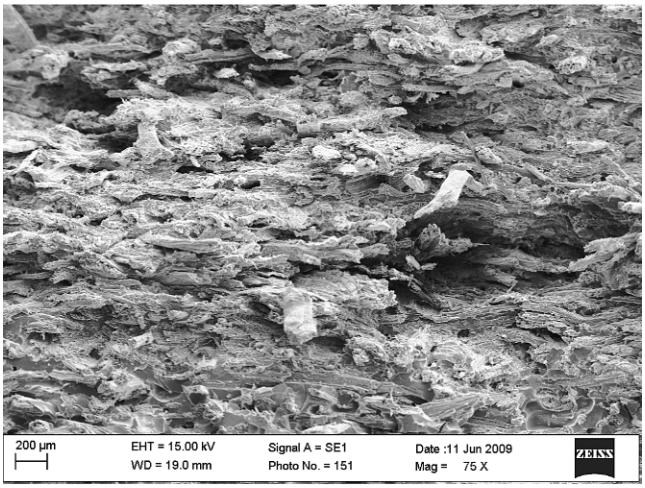

b

Figure 5.—A fracture surface of one kenaf bast fiber bundle–reinforced unsaturated polyester composite tensile specimen. (a) Composite failed with fiber breakage (circle) and fiber pullout (arrow) (Du et al. 2010). (b) A fracture surface at low magnification (×75).

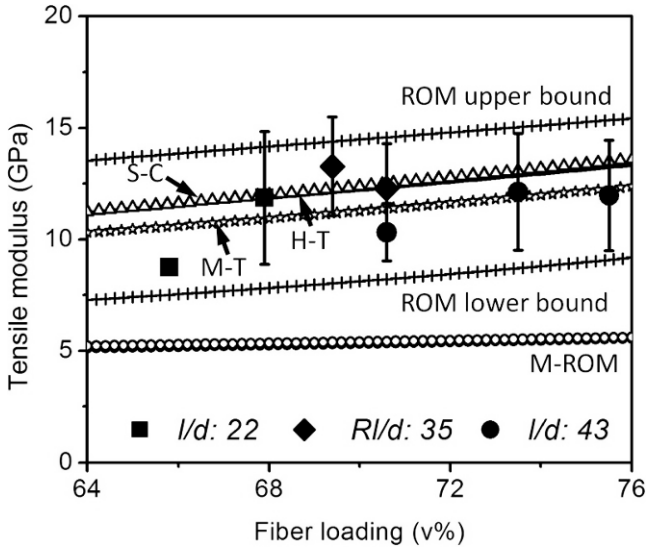

Figure 6.—Kenaf bast fiber bundle (KBFB)–reinforced unsaturated polyester composite experimental and computed tensile moduli reinforced by KBFBs with aspect ratios of 22, 35, and 43, respectively, from bottom to top (overlapped) versus fiber loadings based on the modified rule of mixtures (m-ROM), Halpin–Tsai (H-T), Mori–Tanaka (M-T), and Self-Consistent (S-C) models. v% = percent by volume.

All models showed that the composite tensile moduli increased gradually with increasing fiber loadings, while the m-ROM suggested the lowest dependency of moduli on fiber loadings (Fig. 6). In this work, fiber loadings as high as 75 percent (vol/vol) still resulted in an improvement in the natural fiber–reinforced composite tensile moduli.

The predicted composite tensile moduli obtained using the Halpin–Tsai, Mori–Tanaka, Self-Consistent, and m-ROM models were insensitive to changes in fiber aspect ratio in the range 20 to 40 (Fig. 6). Figure 7 contains a plot of the calculated tensile moduli based on the Halpin–Tsai model as a function of fiber aspect ratio for a number of different fiber loadings. As can be seen from the figure (Fig. 7), the composite moduli asymptotically approach a constant value for a given fiber loading once the fiber aspect ratio exceeds 15.

As an aside, the differences in the measured and predicted elastic properties may be attributable to a number of factors including fiber waviness, poor fiber–matrix adhesion, fiber crushing, etc. (Fig. 5). Such influences may lead to a decrease in the experimentally observed elastic moduli and may contribute to the intrinsic scatter in the experimental data. Yu et al. (in press) developed Mori–Tanaka and Self-Consistent models for predicting effective elastic properties for composites containing hollow wavy fibers surrounded by an arbitrary number of interphase layers; crushed fibers can readily be approximated using noncircular fiber cross-sections. Such approaches may result in an improvement in the predicted stiffness properties provided that the degree of fiber waviness, statistical distribution of fiber cross-section geometries, and fiber–matrix interphase properties were well characterized for the KBFB-reinforced UPE composites considered here. This may be the focus of future work.

Composite tensile strengths were predicted using the Kelly–Tyson (Kelly and Tyson 1965) and Bowyer–Bader (Bowyer and Bader 1972) models that incorporated fiber aspect ratios and loadings. The Kelly–Tyson Model composite strength model may be expressed as

$$\sigma_c = \sigma_f \eta_\theta \eta_l V_f + E_m \varepsilon_c (1 - V_f) \tag{14}$$

where σ_c is the ultimate composite tensile strength, σ_f is the fiber tensile strength, E_m is the matrix tensile modulus, ε_c is the composite ultimate tensile strain, η_θ is the fiber orientation factor whose values may lie between 0.167 and 1, and η_l is the fiber length factor,

$$\eta_l = 1 - L_c/(2L), \; L > L_c \tag{15}$$

$$\eta_l = L/(2L_c), \; L < L_c \tag{16}$$

where L is the fiber length and L_c is the critical fiber length in a matrix. When fibers are randomly aligned in a two-dimensional mat, then $\eta_\theta = 1/3$ (Cox 1952).

The critical fiber length, i.e., the length that is necessary for the maximum stress in the fiber to reach the fiber fracture

Table 3.—Relative errors between composite experimental and theoretical Young's modulus values.

Fiber			Composite tensile modulus				
	Loading		Experiment, mean (SD) (GPa)	Predicted (GPa)[a]			
Aspect ratio	wt%	vol%		H-T	M-T	S-C	m-ROM
22	56.7	65.8	8.8 (—)	11.5 (31)	10.6 (21)	11.6 (32)	5.2 (−41)
22	59.1	67.9	11.9 (2.99)	11.8 (0)	10.9 (−8)	12.0 (1)	5.3 (−56)
35	60.8	69.4	13.3 (2.22)	12.2 (−8)	11.2 (−16)	12.3 (−8)	5.4 (−60)
35	62.0	70.6	12.3 (2.00)	12.4 (1)	11.4 (−7)	12.5 (2)	5.4 (−56)
43	62.0	70.6	10.3 (1.28)	12.4 (20)	11.4 (10)	12.5 (21)	5.4 (−47)
43	65.3	73.5	12.1 (2.63)	12.9 (6)	11.9 (−2)	13.1 (8)	5.5 (−55)
43	67.7	75.5	12.0 (2.48)	13.3 (11)	12.3 (3)	13.5 (13)	5.6 (−53)

[a] H-T = Halpin–Tsai; M-T = Mori–Tanaka; S-C = Self-Consistent; m-ROM = modified rule of mixtures. In the predicted tensile modulus, values in parentheses are relative errors (expressed as percentages) between predicted and experimental values.

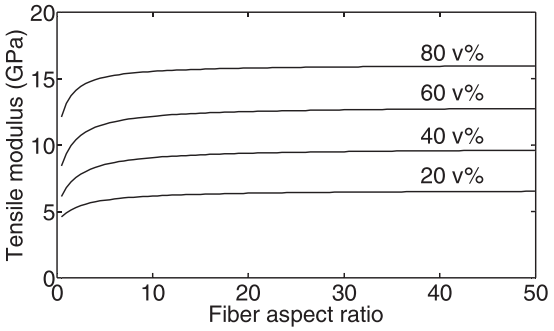

Figure 7.—Kenaf bast fiber bundle–reinforced unsaturated polyester composite theoretical longitudinal tensile moduli computed by the Halpin–Tsai model versus fiber aspect ratios at four fiber loading levels. v% = percent by volume.

stress, σ_f, may be determined using (Kelly and Tyson 1965):

$$L_c = \sigma_f r / \tau_{m-f} \quad (17)$$

where r is the fiber radius and $\tau_{m\text{-}f}$ is the fiber–matrix shear bonding strength. In this study, the shear bonding strength was found to be 6.36 MPa. Therefore, the KBFB critical length with the UPE matrix is 1.61 mm. The average fiber lengths from each fiber batch were used in the strength determination. The Bowyer–Bader composite strength model takes into account variable fiber lengths:

$$\sigma_c = \eta_\theta \int_0^{L_c} \frac{\tau x V_x}{2r}\, dx + \eta_\theta \int_{L_c}^{+\infty} E_f \varepsilon_c \left(1 - \frac{E_f \varepsilon_c r}{2x\tau}\right) V_x\, dx + E_m \varepsilon_c (1 - V_f) \quad (18)$$

where r is the radius of fibers and τ is the fiber–matrix shear strength. The volume fraction, V_x, of fibers of lengths x may be expressed using a two-parameter Weibull distribution model:

$$V_x(x) = \frac{k}{\lambda}\left(\frac{x}{\lambda}\right)^{k-1} \exp\left[-\left(\frac{x}{\lambda}\right)^k\right] \quad (19)$$

Table 4.—Estimated scale and shape parameters of fiber length distributions from three kenaf bast fiber bundle batches.

	Shortest	Median	Longest
k	2.825	2.235	2.509
λ	1.932	3.114	3.803

where k and λ are shape and scale parameters, respectively. The shape and scale parameters were determined from the lengths of 50 randomly selected specimens from each KBFB batch. Table 4 summarizes the estimated parameters used in the composite strength computations.

The predicted composite tensile strengths obtained using the Kelly–Tyson model and experimental values are plotted as a function of fiber loading in Figure 8. Both the measured and predicted strengths increased somewhat with increasing fiber loadings. The Kelly–Tyson model significantly underestimated the observed strengths for composites with average aspect ratio of 22 (average error, −19%). At higher fiber aspect ratios (l/d = 35, 43), the predicted strengths better approximated the observed values (average errors, −5% and 2.6%, respectively). The measured composite strengths as well as predicted values obtained using the Kelly–Tyson and Bowyer–Bader models are listed in Table 5. The Bower–Bader model tended to underestimate the measured strengths for each aspect ratio (l/d = 22, 35, 43) with average errors of −32.5, −20.5, and −10.7 percent, respectively. Similar to the Kelly–Tyson model, the relative

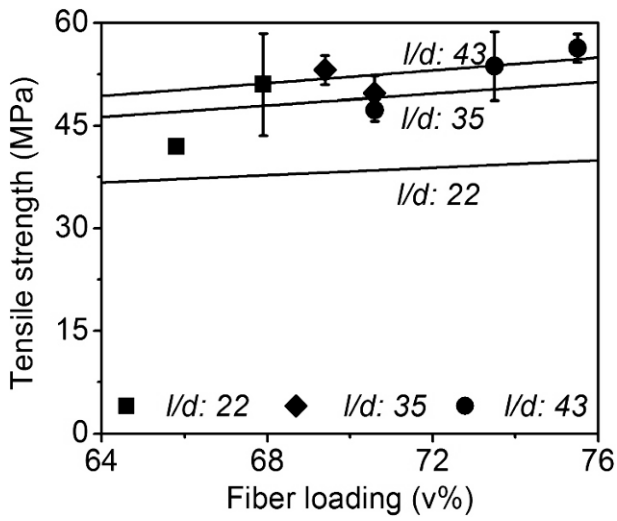

Figure 8.—Kenaf bast fiber bundle (KBFB)–reinforced unsaturated polyester composite experimental and computed tensile strengths versus fiber loadings. The three curves are computed by the Kelly–Tyson model for composites reinforced by KBFBs with aspect ratios of 20, 30, and 40, respectively, from bottom to top. v% = percent by volume.

Table 5.—Relative errors between composite experimental and theoretical tensile strength values.

Fiber			Composite tensile strength		
	Loading		Experiment, mean (SD) (MPa)	Predicted (GPa)[a]	
Aspect ratio	wt%	vol%		Kelly–Tyson	Bower–Bader
22	56.7	65.8	42.0 (—)	37.1 (−12)	30.8 (−27)
22	59.1	67.9	51.0 (7.42)	37.6 (−26)	31.6 (−38)
35	60.8	69.4	53.1 (2.11)	48.6 (−9)	40.6 (−24)
35	62.0	70.6	49.7 (2.60)	49.0 (−1)	41.1 (−17)
43	62.0	70.6	47.3 (1.63)	52.3 (11)	45.2 (−4)
43	65.3	73.5	53.7 (5.02)	53.7 (0)	46.8 (−13)
43	67.7	75.5	56.3 (2.09)	54.6 (−3)	47.9 (−15)

[a] In the predicted tensile strength, values in parentheses are relative errors (expressed as percentages) between predicted and experimental values.

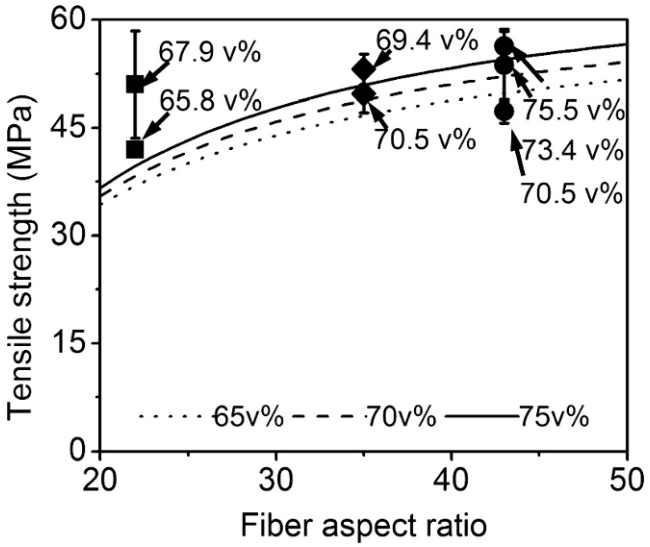

Figure 9.—Kenaf bast fiber bundle–reinforced unsaturated polyester composite experimental and calculated tensile strengths versus fiber aspect ratios. The three curves were computed by the Kelly–Tyson model for composites with fiber loadings of 65, 70, and 75 percent (by volume [v%]), respectively, from bottom to top.

errors associated with the Bower–Bader model decreased with increasing fiber ratios.

The measured composite strengths in this study, in general, increased with increasing fiber loadings up to 75 percent (vol/vol; Fig. 8). Takagi and Ichihara (2004) reported composite tensile strengths increased as the fiber loading increased from 0 to 50 percent (wt/wt). Devi et al. (1997) reported increasing tensile strengths as the fiber loadings increased from 10 to 40 percent (wt/wt). However, decreasing tensile strengths at higher fiber loadings were also reported (Baiardo et al. 2004, Shibata et al. 2006, Xue et al. 2007).

Figure 9 shows a plot of the measured composite tensile strengths as a function of fiber aspect ratio, as well as calculated values based upon the Kelly–Tyson model for 65, 70, and 75 percent (vol/vol), respectively. The strengths generally increased with increasing fiber aspect ratios as well as fiber loadings. The calculated results suggest that the composite strength values asymptotically approach a constant value for a given fiber loading as the aspect ratio becomes large (corresponding to the continuous fiber solution). Further investigation on the effect of fiber aspect ratio on composite tensile strengths is needed due to the lack of experimental results at fixed fiber loading levels.

Summary and Conclusions

Tensile properties of KBFB-reinforced UPE composites with high fiber loadings up to 75 percent (vol/vol) were studied. Both composite tensile moduli and strengths consistently increased with increasing fiber loading. The measured composite tensile moduli correlated reasonably well with predictions obtained using the Halpin–Tsai, the Mori–Tanaka, and the Self-Consistent models. The measured and calculated composite tensile moduli were insensitive to fiber aspect ratios in the range of 22 to 45. Composite tensile strengths were reasonably computed by the Kelly–Tyson model at higher fiber aspect ratio levels. In general, composite strengths increased with both increasing fiber aspect ratio and loadings. This study confirms that high fiber loading in natural fiber–reinforced composites can result in improved composite tensile properties, while reducing composite material costs due to lower petroleum-based polymer content. With increased improvement in mechanical properties, natural fiber composites may be viable replacement materials for traditional glass fiber composites in automotive structural applications.

Acknowledgments

The authors express appreciation for financial support of this work by the US Department of Energy, Center for Advanced Vehicular Systems and Forest Product Department at Mississippi State University (Grant No. DE-FC26-06NT42755). We express special gratitude to Kengro Corporation, Tailored Chemical Products Inc., and Ashland Chemical Company for donated materials.

Literature Cited

Abu Bakar, M. A., S. Ahmad, and W. Kuntjoro. 2010. The mechanical properties of treated and untreated kenaf fibre reinforced epoxy composite. *J. Biobased Mater. Bioenergy* 4(2):159–163.

Agarwal, B. D., L. J. Broutman, and K. Chandrashekhara. 2006. Analysis and Performance of Fiber Composites. John Wiley & Sons, Inc., Hoboken, New Jersey.

ASTM International. 2003. Standard test method for tensile strength and Young's modulus of fibers. C1557-03. *In:* Annual Book of ASTM Standards. Vol. 15.01. ASTM International, West Conshohocken, Pennsylvania.

ASTM International. 2004. Standard test method for tensile properties of plastics. D638–03. *In:* Annual Book of ASTM Standards. Vol. 08.01, Plastics (I). ASTM International, West Conshohocken, Pennsylvania.

Baiardo, M., E. Zini, and M. Scandola. 2004. Flax fibre-polyester composites. *Compos. Part A Appl. Sci. Manuf.* 35(6):703–710.

Benveniste, Y. 1987. A new approach to the application of Mori-Tanaka's theory in composite materials. *Mech. Mater*. 6:147–157.

Bowyer, W. H. and M. G. Bader. 1972. On the reinforcement of thermoplastics by imperfectly aligned discontinuous fibres. *J. Mater. Sci*. 7(11):1315–1321.

Brandrup, J. and E. H. Immergut. 1989. Polymer Handbook. 3rd ed. John Wiley & Sons Inc., New York.

Cox, H. L. 1952. The elasticity and strength of paper and other fibrous materials. *Br. J. Appl. Phys*. 3(3):72–79.

Devi, L. U., S. S. Bhagawan, and S. Thomas. 1997. Mechanical properties of pineapple leaf fiber-reinforced polyester composites. *J. Appl. Polym. Sci*. 64(9):1739–1748.

Du, Y., J. Zhang, H. Toghiani, T. E. Lacy, Jr., Y. Xue, M. F. Horstemeyer, and C. U. Pittman, Jr. 2010. Kenaf bast fiber bundle–reinforced unsaturated polyester composites. I: Processing techniques for high kenaf fiber loading. *Forest Prod. J*. 60(3):289–295.

Du, Y., J. Zhang, and Y. Xue. 2008. Temperature-duration effects on tensile properties of kenaf bast fiber bundles. *Forest Prod. J*. 58(9): 59–65.

Eshelby, J. 1957. The determination of the elastic field of an ellipsoidal inclusion. *Proc. R. Soc. Lond*. 241(1226):376–396.

Fisher, F. T. 2002. Nanomechanics and the viscoelastic behavior of carbon nanotube-reinforced polymers. Doctoral dissertation. Northwestern University, Evanston, Illinois.

Halpin, J. C. 1969. Stiffness and expansion estimates for oriented short fiber composites. *J. Compos. Mater*. 3:732–734.

Haneefa, A., P. Bindu, I. Aravind, and S. Thomas. 2008. Studies on tensile and flexural properties of short banana/glass hybrid fiber reinforced polystyrene composites. *J. Compos. Mater*. 42(15): 1471–1489.

Hill, R. 1965. A self-consistent mechanics of composite materials. *J. Mech. Phys. Solids* 13(4):213–222.

Hirsch, T. J. 1962. Modulus of elasticity of concrete affected by elastic moduli of cement paste matrix and aggregate. *J. Am. Concrete Inst*. 59(3):427–451.

Holbery, J. and D. Houston. 2006. Natural fiber reinforced polymer composites in automotive applications. *J. Mater*. 58(11):80–86.

Joseph, P. V., G. Mathew, K. Joseph, S. Thomas, and P. Pradeep. 2003. Mechanical properties of short sisal fiber-reinforced polypropylene composites: Comparison of experimental data with theoretical predictions. *J. Appl. Polym. Sci*. 88(3):602–611.

Kelly, A. and W. R. Tyson. 1965. Tensile properties of fiber-reinforced metals: copper/tungsten and copper/molybdenum. *J. Mech. Phys. Solids* 13(6):329–338.

Liu, W., L. T. Drzal, A. K. Mohanty, and M. Misra. 2007. Influence of processing methods and fiber length on physical properties of kenaf fiber reinforced soy based biocomposites. *Compos. Part B* 38(3):352–359.

Mark, H. F. 2004. Vinyl acetate polymers. *In:* Encyclopedia of Polymer Science and Technology. Vol. 12. 3rd ed. Wiley-Interscience, Hoboken, New Jersey. 424 pp.

Mori, T. and K. Tanaka. 1973. Average stress in matrix and average elastic energy of materials with misfitting inclusions. *Acta Metallurgica* 21(5):571–574.

Mura, T. 1991. Micromechanics of Defects in Solids. 2nd ed. Kluwer Academic Publishers, The Netherlands. pp. 10–73.

Nemat-Nasser, S. and M. Hori. 1993. Micromechanics: Overall Properties of Heterogeneous Materials. North-Holland, Amsterdam. pp. 368–386.

Nielsen, L. E. 1970. Generalized equation for the elastic moduli of composite materials. *J. Appl. Phys*. 41(11):4626–4627.

Nielsen, L. E. and P. E. Chen. 1968. Young's modulus of composites filled randomly oriented fibers. *J. Mater*. 3(2):352–358.

Ochi, S. 2008. Mechanical properties of kenaf fibers and kenaf/PLA composites. *Mech. Mater*. 40(4–5):446–452.

Özturk, S. 2010. Effect of fiber loading on the mechanical properties of kenaf and fiberfrax fiber-reinforced phenol-formaldehyde composites. *J. Compos. Mater*. 44(19):2265–2288.

Pascault, J.-P., H. Sautereau, and J. Verdu. 2002. Thermosetting Polymers. Marcel Dekker, Inc., New York.

Qu, J. and M. Cherkaoui. 2006. Fundamental of Micromechanics of Solids. John Wiley & Sons, Inc., Hoboken, New Jersey.

Shibata, S., I. Fukumoto, and Y. Cao. 2006. Effects of fiber compression and length distribution on the flexural properties f short kenaf fiber-reinforced biodegradable composites. *Polym. Compos*. 27(2):170–176.

Takagi, H. and Y. Ichihara. 2004. Effect of fiber length on mechanical properties of ''green'' composites using a starch-based resin and short bamboo fibers. *JSME Int. J. Ser. A* 47(4):551–555.

Xue, Y., D. R. Veazie, C. Glinsey, M. F. Horstemeyer, and R. M. Rowell. 2007. Environmental effects on the mechanical and thermomechanical properties of aspen fiber-polypropylene composites. *Compos. Part B Eng*. 38(2):152–158.

Yu, J., T. E. Lacy, H. Toghiani, and C. U. Pittman, Jr. Classical micromechanics modeling of nanoreinforced composites with carbon nanofibers and interphase. *J. Compos. Mater*. (in press).